elastix: A Toolbox for Intensity-Based Medical Image Registration

Stefan Klein†, Marius Staring†*, Keelin Murphy, Max A. Viergever, and Josien P. W. Pluim

***Abstract*—Medical image registration is an important task in medical image processing. It refers to the process of aligning data sets, possibly from different modalities (e.g., magnetic resonance and computed tomography), different time points (e.g., follow-up scans), and/or different subjects (in case of population studies). A large number of methods for image registration are described in the literature. Unfortunately, there is not one method that works for all applications. We have therefore developed elastix, a publicly available computer program for intensity-based medical image registration. The software consists of a collection of algorithms that are commonly used to solve medical image registration problems. The modular design of elastix allows the user to quickly configure, test, and compare different registration methods for a specific application. The command-line interface enables automated processing of large numbers of data sets, by means of scripting. The usage of elastix for comparing different registration methods is illustrated with three example experiments, in which individual components of the registration method are varied.**

***Index Terms*—elastix, image registration, medical imaging, open source, software.**

I. Introduction

IMAGE registration is a frequently used technique in medical image processing. It is the task of finding the spatial relationship between two or more images. Areas of application include the alignment of data sets from different modalities [1], comparison of follow-up scans to a base-line scan [2], alignment of pre- and post-contrast images [2]–[4], updating treatment plans for radiotherapy and surgery [5], [6], atlas-based segmentation [7]–[13], creating models of anatomy [14], and aligning training images for classification [15], [16].

Manuscript received August 14, 2009; revised October 22, 2009; accepted October 22, 2009. First published November 17, 2009; current version published January 04, 2010. This work was supported by the Netherlands Organisation for Scientific Research (NWO). This work also benefited from the use of the Insight Segmentation and Registration Toolkit (ITK), an open source software package developed as an initiative of the U.S. National Library of Medicine and available at http://www.itk.org. †In alphabetical order. Both authors contributed equally. *Asterisk indicates corresponding author.*

S. Klein was with the University Medical Center Utrecht, Image Sciences Institute, 3508 GA Utrecht, The Netherlands. He is now with the Biomedical Imaging Group Rotterdam, Departments of Radiology and Medical Informatics, Erasmus MC, Rotterdam, The Netherlands (e-mail: s.klein@erasmusmc.nl).

*M. Staring was with the University Medical Center Utrecht, Image Sciences Institute, 3508 GA Utrecht, The Netherlands. He is now with the Division of Image Processing, Department of Radiology, Leiden University Medical Centre, 2333 ZA Leiden, The Netherlands (e-mail: m.staring@lumc.nl).

K. Murphy, M. A. Viergever, and J. P. W. Pluim are with the University Medical Center Utrecht, Image Sciences Institute, 3508 GA Utrecht, The Netherlands (e-mail: keelin@isi.uu.nl; max@isi.uu.nl; josien@isi.uu.nl).

Digital Object Identifier 10.1109/TMI.2009.2035616

In registration, one image, which is called the *moving image* $I_M(\boldsymbol{x})$, is deformed to fit the other image, the *fixed image* $I_F(\boldsymbol{x})$. In other words, registration is the problem of finding a *coordinate transformation* $\boldsymbol{T}(\boldsymbol{x})$ that makes $I_M(\boldsymbol{T}(\boldsymbol{x}))$ spatially aligned with $I_F(\boldsymbol{x})$. The quality of alignment is defined by a cost function $\mathcal{C}(\boldsymbol{T}; I_F, I_M)$. The optimal coordinate transformation is estimated by minimizing the cost function with respect to $\boldsymbol{T}$, usually by means of an iterative optimization method embedded in a hierarchical (multiresolution) scheme. The registration problem is not always properly defined, for instance when registering one cerebral cortex to that of another patient. Extensive reviews on the subject of image registration are given in [17]–[22].

Application of an image registration method requires many choices to be made, such as the optimization method, the multiresolution strategy, the method of image interpolation to evaluate $I_M(\boldsymbol{T}(\boldsymbol{x}))$, the coordinate transformation model, and the definition of the cost function. Several possibilities for the optimization method are discussed in [23] and [24]. An overview of multiresolution strategies is given in [19]. Various image interpolation methods are compared in [25]. The degrees-of-freedom of the coordinate transformation $\boldsymbol{T}$ determine the types of deformations that can be recovered. Whereas in many applications it may be sufficient to consider only rigid transformations (global translations and rotations) [26], [27], frequently a more flexible transformation model is needed, allowing for local deformations [1], [3], [28]–[39]. For the cost function $\mathcal{C}$ many options have been proposed in the literature. Commonly used intensity-based cost functions are the mean squared difference (MSD) [40], [41], normalized correlation (NC) [42], [43], mutual information (MI) [26], [44]–[46], and normalized mutual information (NMI) [4], [7], [47]. Sometimes, a regularization term is added to the cost function, in order to penalize undesired deformations [2], [4], [35]. In medical image processing research it is often necessary to compare several options for each of the registration components. Given the large number of choices, this can be a tedious procedure.

To facilitate the research on medical image registration and to simplify its application, we have developed an open source software package: elastix. The elastix software has a modular design, including several optimization methods, multiresolution schemes, interpolators, transformation models, and cost functions. This allows the user to quickly compare different registration methods, in order to select a satisfactory configuration for a specific application. elastix has a command-line interface, which enables automated processing of large numbers of data sets, by means of scripting. The software is built upon a

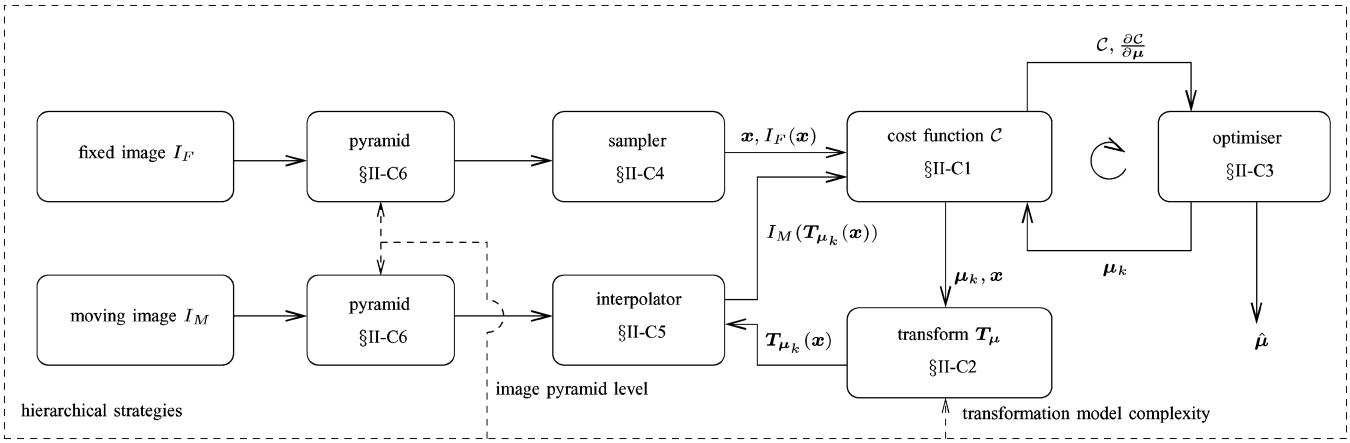

Fig. 1. Basic registration components. The scheme is an extended version of the scheme introduced in [48]. Each component is accompanied by a section number where more information can be found. Dashed box around the complete scheme represents the various hierarchical strategies, which can affect all components; see Section II-C-6.

widely used open source library for medical image processing, the Insight Toolkit (ITK) [48].

In Section II, the general registration framework of `elastix` is discussed, key features of the software are presented, and an overview of the available registration components is given. In Section III, three examples of applications that can be handled with the software are given. In these experiments, the influence of three important registration components is demonstrated. Section IV presents several guidelines for the use of `elastix`. The paper ends with a discussion (Section V) and the conclusions (Section VI).

II. Image Registration With Elastix

A. Registration Framework

Mathematically, the registration problem is formulated as an optimization problem in which the cost function $\mathcal{C}$ is minimized with respect to $\boldsymbol{T}$. The `elastix` software is based on a parametric approach, meaning that the number of possible transformations is limited by introducing a parametrization of the transformation. The optimization problem reads

$$\hat{\boldsymbol{\mu}} = \arg\min_{\boldsymbol{\mu}} \mathcal{C}(\boldsymbol{T}_{\boldsymbol{\mu}}; I_F, I_M) \tag{1}$$

where the subscript $\boldsymbol{\mu}$ indicates that the transform has been parameterized. The vector $\boldsymbol{\mu}$ contains the transformation parameters. The reader is referred to [21] and [35] for an overview on nonparametric methods. The minimization problem (1) is solved with an iterative optimization method, usually in a multiresolution setting. A schematic overview of the basic registration components and their relations is given in Fig. 1, which is a slightly extended version of the scheme introduced in [48]. A detailed explanation of the various components is given in Section II-C.

B. Software Characteristics

The `elastix` software is structured according to the block scheme of Fig. 1. For each component (transform, cost function, etc.) several choices are available. The user can configure a registration algorithm by specifying the names of the desired components in a parameter text file. Additional settings that some components may require can also be entered in this parameter file. Fixed and moving image file names are supplied as command-line arguments, so that multiple image pairs can be registered using the same parameter settings. An example of usage is given in the Appendix. Both 2-D and 3-D images are supported.

All output of the registration, such as the deformed moving image $I_M(\boldsymbol{T}_{\hat{\boldsymbol{\mu}}}(\boldsymbol{x}))$ and intermediate progress information, is saved to disk. It is often necessary to apply the resulting transformation $\boldsymbol{T}_{\hat{\boldsymbol{\mu}}}$ to data sets other than the moving image. For example, in atlas-based segmentation methods [7], [8] the transformation is applied to a segmentation (label image) of the moving image. To that end, `elastix` outputs a text file that describes the transformation $\boldsymbol{T}_{\hat{\boldsymbol{\mu}}}$. This text file can subsequently be passed to an accompanying program, called `transformix`, together with the image to be deformed. This program can also be used to evaluate the transformation at user-defined points, or to generate the deformation field.

A large part of the `elastix` code is based on the ITK [48]. The use of the ITK implies that the low-level functionality (image classes, memory allocation, etc.) is thoroughly tested. Naturally, all image formats supported by the ITK are supported by `elastix` as well. The C++ source code can be compiled on multiple operating systems (Windows XP, Linux, Mac OS X), using various compilers (MS Visual Studio up to version 2008, GCC up to version 4.3), and supports both 32 and 64 bit systems. In addition to the existing ITK image registration classes, `elastix` implements new functionality. The most important enhancements are listed in Table I.

The `elastix` source code consists roughly of two layers, both written in C++: A) ITK-style classes that implement image registration functionality, and B) `elastix` wrappers that take care of reading and setting parameters, instantiating and connecting components, saving (intermediate) results, and similar "administrative" tasks. The modular design enables adding new components, without changing the `elastix` core. Adding a new component starts by creating the layer A class, which can

TABLE I
THE MOST IMPORTANT ENHANCEMENTS AND ADDITIONS IN elastix, COMPARED TO THE ITK

- A modular framework for sampling strategies.
- Several new optimisers: Kiefer-Wolfowitz, Robbins-Monro, adaptive stochastic gradient descent, evolutionary strategy.
- Complete rework of existing ITK optimisers, adding more user control and better error handling: quasi-Newton, nonlinear conjugate gradient.
- Several new or more flexible cost functions: (normalised) mutual information, implemented with Parzen windowing similar to [45], multifeature α-mutual information, bending energy penalty term, rigidity penalty term.
- The ability to concatenate any number of geometric transformations.
- The transformations support computation of not only $\partial \boldsymbol{T}/\partial \boldsymbol{\mu}$, but also of spatial derivatives $\partial \boldsymbol{T}/\partial \boldsymbol{x}$ and $\partial^2 \boldsymbol{T}/\partial \boldsymbol{x}^2$, and their derivatives to $\boldsymbol{\mu}$, frequently required for the computation of regularisation terms.
- The compact support of certain transformations, i.e. the fact that the derivative $\partial \boldsymbol{T}/\partial \boldsymbol{\mu}$ is zero for many of its indices, is in the ITK currently only exploited for the combination of mutual information and a B-spline transformation. In elastix this is integrated in a generic way (not only for the combination of mutual information and B-splines).
- Linear combinations of cost functions, instead of just a single cost function.
- A Gaussian pyramid without downsampling.

be compiled and tested independent of layer B. Subsequently, a small layer B wrapper needs to be written, which connects the layer A class to the other parts of elastix.

Executables and source code are publicly available online[1] under the BSD license, which allows free academic and commercial use and permits modification of the source code. A manual for elastix and an example of usage can also be downloaded. The manual includes an example parameter file, describes in detail the various options that can be specified, and provides recommendations for image registration. The manual also contains information about elastix's more advanced registration possibilities, not treated in this paper, such as the registration of multispectral data. In addition, we created a "parameter file database," which is a collection of parameter files that proved successful, together with a short description of the clinical application for which they were used. The parameter file database can be found through the website[2] and elastix-users are encouraged to upload their own settings. A default parameter file can also be found here.

C. Registration Components

In the following subsections, more information is given about each component of the block scheme in Fig. 1.

1) Cost Function: The cost function $\mathcal{C}$ measures the similarity between the fixed image and the transformed moving image. An example is the MSD

$$\mathrm{MSD}(\boldsymbol{T}_{\boldsymbol{\mu}}; I_F, I_M) = \frac{1}{N} \sum_{\boldsymbol{x} \in \Omega_F} \left(I_F(\boldsymbol{x}) - I_M\left(\boldsymbol{T}_{\boldsymbol{\mu}}(\boldsymbol{x})\right)\right)^2 \quad (2)$$

where Ω_F denotes the fixed image domain, and N the number of voxels $\boldsymbol{x}$ sampled from the fixed image domain. The sampler, which is responsible for selecting the samples $\boldsymbol{x}$, is discussed in more detail in Section II-C-4.

[1]http://elastix.isi.uu.nl

[2]http://elastix.isi.uu.nl/wiki.php

The following metrics are currently supported by elastix: mean square difference (MSD), normalized correlation (NC), mutual information (MI), normalized MI (NMI), α-MI [49], [50], and the κ-statistic [51]. MSD is only suited for two images with equal intensities, i.e., for images from the same modality. NC is less strict, it assumes an affine relation between the intensity values of the fixed and moving image. MI, NMI, and α-MI assume only a statistical relation between the intensities of the images. They are therefore suited not only for monomodal, but also for multimodal image pairs. The κ-statistic can be used for registering binary images. It measures the overlap of objects in the images. For each of the metrics above, a localized version can be constructed, as explained in [8], by selecting the appropriate sampler. This is described in Section II-C-4.

Parameters such as the number of bins of the joint histogram, needed for MI and NMI, can be set in the aforementioned parameter file.

When a nonrigid transformation model is used, a regularization term that penalizes undesired deformations can be added to the cost function. An example is the incompressibility constraint described by [4], which penalizes compression and expansion of structures. Other examples of regularization terms are the bending energy of a thin plate [3] and the rigidity penalty term [2]. elastix supports these constraints.

2) Transformation: The parametrization of the coordinate transformation $\boldsymbol{T}_{\boldsymbol{\mu}}$ determines the degrees-of-freedom of the deformation. An example is the affine transformation model, which allows for translation, rotation, scaling and skew of the images

$$\boldsymbol{T}_{\boldsymbol{\mu}}(\boldsymbol{x}) = A\boldsymbol{x} + \boldsymbol{t} \quad (3)$$

where A is a matrix and $\boldsymbol{t}$ represents the translation vector. The parameter vector $\boldsymbol{\mu}$ is formed by the matrix elements a_{ij} and the translation vector. In 2-D, this gives a vector of dimension 6: $\boldsymbol{\mu} = (a_{11}, a_{12}, a_{21}, a_{22}, t_x, t_y)^T$. In 3-D, $\boldsymbol{\mu}$ consists of 9 matrix elements and 3 translational components.

The following transformation models are currently supported by elastix, with the number of degrees-of-freedom (dimension of $\boldsymbol{\mu}$) between brackets: translation (3), rigid (translation and rotation, 6), similarity (rigid plus isotropic scaling, 7), affine (12), and nonrigid (varying size of $\boldsymbol{\mu}$). In the literature, several parametric nonrigid transformation models have been proposed [3], [28], [30], [32], [36], [37], each having its own advantages and disadvantages. In elastix a *B*-spline representation [3] has been implemented and several physics-based spline models [30], [52], such as the thin-plate spline and the elastic body spline. The *B*-spline transformation is modelled as a weighted sum of *B*-spline basis functions, placed on a uniform control point grid. The *B*-spline basis functions have local support [53], which is beneficial for fast computation. The flexibility of the deformation is defined by the resolution of the control point grid, which has to be supplied by the user via the parameter file. Section III-A demonstrates the effect of using different control point resolutions for an example application. The physics-based spline transformation allows the user to place control points at arbitrary positions, not necessarily on a uniform grid. Lastly, elastix includes a transformation

that is modelled as a weighted combination of user-specified transformations: $\boldsymbol{T}_{\boldsymbol{\mu}}(\boldsymbol{x}) = \sum_i w_i \boldsymbol{T}_i(\boldsymbol{x})$. The weights w_i form the parameter vector $\boldsymbol{\mu}$. The subtransforms $\boldsymbol{T}_i(\boldsymbol{x})$ may for example follow from a statistical deformation model, obtained by principal component analysis [54].

The aforementioned regularization term in the cost function is often expressed in terms of first- and second-order spatial derivatives of the transformation $\partial \boldsymbol{T}/\partial \boldsymbol{x}$ and $\partial^2 \boldsymbol{T}/\partial \boldsymbol{x}^2$ [2]–[4]. The modular framework of the ITK was extended to support these derivatives, together with their derivatives to $\boldsymbol{\mu}$ required for gradient-based optimization routines.

Frequently, nonrigid registration must be preceded by a rigid or affine registration, in order to achieve a rough initial alignment. elastix supports the concatenation of any sequence of transforms. The user may also supply an initial transformation, determined in advance by the user. It can be expressed as one of the available transformations, or as a dense deformation field vector image. The transformation may for example be derived (in external software) from a set of manually clicked corresponding points.

3) Optimization: To solve (1), an iterative optimization procedure is employed. In every iteration k, the current transformation parameters $\boldsymbol{\mu}_k$ are updated by taking a step in the search direction $\boldsymbol{d}_k$

$$\boldsymbol{\mu}_{k+1} = \boldsymbol{\mu}_k - a_k \boldsymbol{d}_k \tag{4}$$

with a_k a scalar that determines the step size. A wide range of optimization methods can be formulated in this way, each having different definitions of a_k and $\boldsymbol{d}_k$ [24]. A common choice for the search direction is the derivative of the cost function $\partial \mathcal{C}/\partial \boldsymbol{\mu}$ evaluated at the current position $\boldsymbol{\mu}_k$. In this case, (4) reduces to a gradient descent method.

elastix includes all optimization methods described in [24]: gradient descent, quasi-Newton, nonlinear conjugate gradient (several variants), evolution strategy, and a number of stochastic gradient descent methods (Kiefer–Wolfowitz, Robbins–Monro, and simultaneous perturbation). An exhaustive search routine is also included, which is mainly useful for examining the cost function, as demonstrated in Section III-B. The experimental results in [24] indicate that a stochastic gradient descent method (Robbins–Monro) is a good choice for many applications. It reduces the computation time per iteration by using only a small subset of the fixed image's voxels for computing the cost function derivative. In each iteration, new samples must be selected randomly. This can be realized in elastix by selecting an appropriate sampler, which is explained in the next subsection. A recent extension of the Robbins–Monro algorithm, called adaptive stochastic gradient descent [55], which aims at simplified parameter selection and further acceleration, is also included in elastix.

4) Sampling Strategies: To compute the cost function $\mathcal{C}$ (and its derivative $\partial \mathcal{C}/\partial \boldsymbol{\mu}$) a set of samples $\boldsymbol{x} \in \Omega_F$ needs to be selected, as in (2). The sampler component in Fig. 1 is responsible for this. The most straightforward strategy is to use all voxels from the fixed image, which has as an obvious downside that it is time-consuming for large images. A common approach is to use a subset of voxels, selected on a uniform grid, or sampled randomly. Another strategy is to pick only those points that are located on striking image features, such as edges [56].

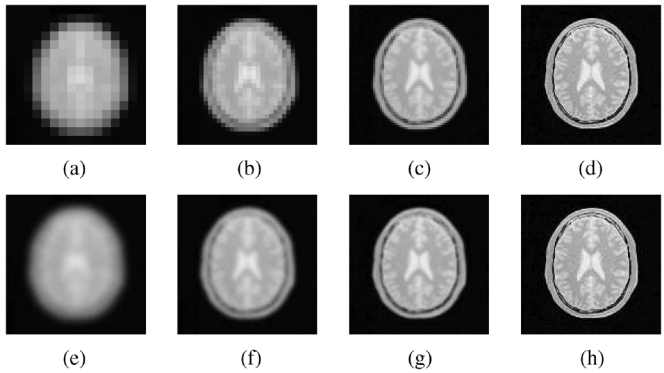

Fig. 2. Two multiresolution strategies using a Gaussian pyramid ($\sigma = 8.0, 4.0, 2.0$ voxels). The top row shows multiresolution with downsampling, the bottom row without. Note that in the top row the number of voxels in each dimension is halved every resolution, but the voxel size is doubled, so physically the images are of the same size. (a) res. 0. (b) res. 1. (c) res. 2. (d) original. (e) res. 0. (f) res. 1. (g) res. 2. (h) original.

elastix currently supports the use of all voxels, a subset of voxels selected on a uniform grid, random sampling of voxels, and random sampling off the voxel grid (at nonvoxel locations). Random sampling off the grid has been shown to improve the smoothness of the cost function [57], [58]. In Section III-B, we demonstrate this effect by comparing several sampling schemes on an example application. For all sampling strategies discussed above, the user may optionally supply a mask image, indicating regions of interest. In this way, one can force the sampler to pick only points near edges in the image, for example.

With random sampling, the elastix user can enforce the selection of new samples in every iteration k of the optimization process. In this way, the stochastic optimization methods described in [24] can be realized. The localized mutual information strategy, presented in [8], can be implemented by letting the sampler pick points in a small neighborhood, instead of from the entire domain Ω_F. A new neighborhood is randomly selected in every iteration of the optimization procedure.

5) Interpolation: For computation of the cost function, the value $I_M(\boldsymbol{T}_{\boldsymbol{\mu}}(\boldsymbol{x}))$ is evaluated at nonvoxel positions, for which intensity interpolation is needed. Several methods for interpolation exist, varying in quality and speed, including nearest neighbor, linear and $\mathcal{N}$th-order *B*-spline interpolation [53], [59]. elastix supports all interpolators mentioned above.

For the fixed image I_F no interpolation is required with most sampling strategies, since the image is sampled at voxel locations. For sampling off the voxel grid, however, an additional interpolator is needed, not depicted in Fig. 1.

6) Hierarchical Strategies: Hierarchical (multiresolution) strategies are an important aspect of image registration. For an extensive overview, the reader is referred to [19]. elastix implements several hierarchical strategies:

- The pyramid components in the block scheme of Fig. 1 represent the multiresolution schemes for the *image data*. Two types of image pyramids are available in elastix: Gaussian pyramids with and without downsampling. Fig. 2 illustrates the difference.

- The second important multiresolution strategy, not apparent from Fig. 1, is the gradual increase of *transformation model* complexity. During nonrigid registration, a hierarchical effect can be realized by starting with a coarse *B*-spline control point resolution and gradually refining the grid in subsequent resolutions [53], thereby introducing the capability to recover more fine-scale deformations. In `elastix`, the *B*-spline control point grid can be refined using any upsampling factor, possibly different for each dimension.
- More generally, many parameter settings can be subjected to a hierarchical strategy in `elastix`. For example, the number of joint histogram bins that is used for computing MI and NMI could be gradually increased, as was suggested in [45].

The third point above is represented by the dashed box around the entire scheme. The first two strategies, regarding image pyramid level and transformation model complexity, are depicted explicitly in Fig. 1 by the dashed arrows originating from the outer box. In Section III-C several multiresolution strategies are compared for the nonrigid registration of computed tomography (CT) chest scans.

III. Experiments and Results

In this section, some applications of `elastix` are described, to illustrate its convenience for configuring, testing, and comparing different registration methods. To illustrate the wide usability of `elastix`, the image data was chosen from different modalities, at different acquisition times, and from different subjects. Three key components of registration were studied: the transformation model in Section III-A, the sampling technique in Section III-B, and the multiresolution strategy in Section III-C. The experiments demonstrate the impact these components can have on the registration results, and therefore stress the importance of a proper configuration for the application at hand.

The `elastix` settings that were used in the following subsections have been made available via the parameter file database, see Section II-B. Exact registration settings for each experiment can be inspected there, and the parameter files can be downloaded for use in other applications.

A. Transformation Models

The effect of the type of transformation was investigated by comparing the registration performance of several transformation models.

To this end, a set of 50 clinical MR scans of the prostate was used, all originating from different patients. The scans were made by the Department of Radiotherapy of the University Medical Center Utrecht, as part of prostate cancer treatment planning. They were acquired on a Philips 3T scanner (Gyroscan NT Intera, Philips Medical Systems, Best, The Netherlands) using a balanced steady-state free precession sequence with fat suppression. The scans had dimensions of $512 \times 512 \times 90$ voxels of size $0.49 \times 0.49 \times 1.0$ mm.

Fifty interpatient registrations were performed by registering each MR scan with its predecessor in the 50-scan series. Interpatient registration of these scans is needed for atlas-based segmentation of the prostate [8]. The registration problem is challenging, since the anatomical variability between subjects is large. Also, the data suffer from several artefacts, as shown in [8]. For our experiments we used the same settings as in [8], with localized MI as a cost function (see Section II-C-4), and a four-level Gaussian image pyramid with downsampling. The following transformation models were compared: translation, rigid, affine, and *B*-spline with different control point spacings: 64, 32, 16, 8, and 4 mm. The result of the registration with translations was only used as an initialization for all other registrations. For the *B*-spline registrations, the control point grid was subjected to a multiresolution scheme: registration starts with a coarse control point resolution; with less smooth versions of the images, the control point resolution is increased accordingly.

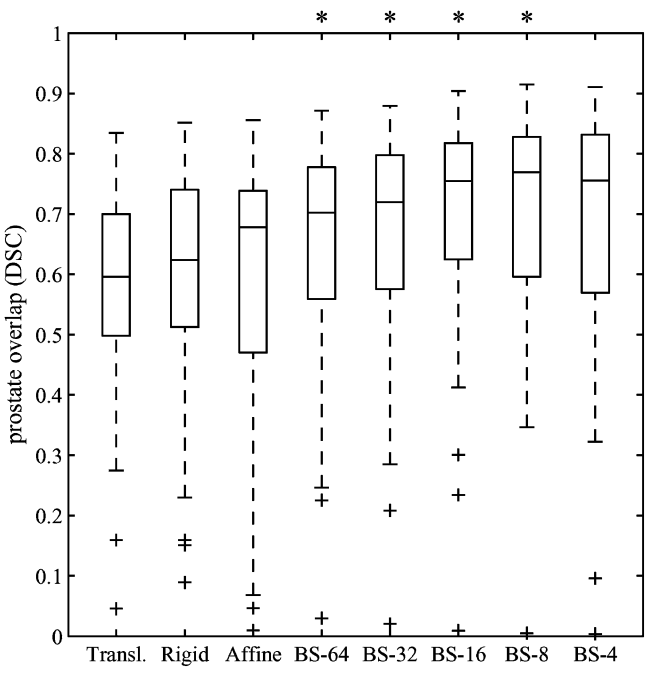

Fig. 3. Effect of the transformation model on the accuracy of registration, measured by the prostate overlap. Abbreviation BS-$\langle sp \rangle$ refers to a *B*-spline transformation with control point spacing sp, in millimeters.

For all images a manual segmentation of the prostate was available, made by an experienced radiation oncologist. After registration with `elastix`, the transformation $\boldsymbol{T}_{\hat{\boldsymbol{\mu}}}$ was applied to the prostate segmentation of the moving image, using `transformix`. The overlap with the segmentation of the fixed image was computed, using the Dice similarity coefficient (DSC) [60]:

$$\mathrm{DSC}(X,Y) = \frac{2|X \cap Y|}{|X| + |Y|} \tag{5}$$

where X and Y represent the two segmentations, and $|\cdot|$ denotes the number of voxels within the segmentation. A DSC of 1 indicates a perfect alignment of the segmentation boundary. A value of 0 means that the prostates had no overlap at all after registration.

The results are presented in Fig. 3. For each transformation model, the DSC values of the 50 MR scans were summarised by a box-and-whiskers plot. A paired, two-sided Wilcoxon test

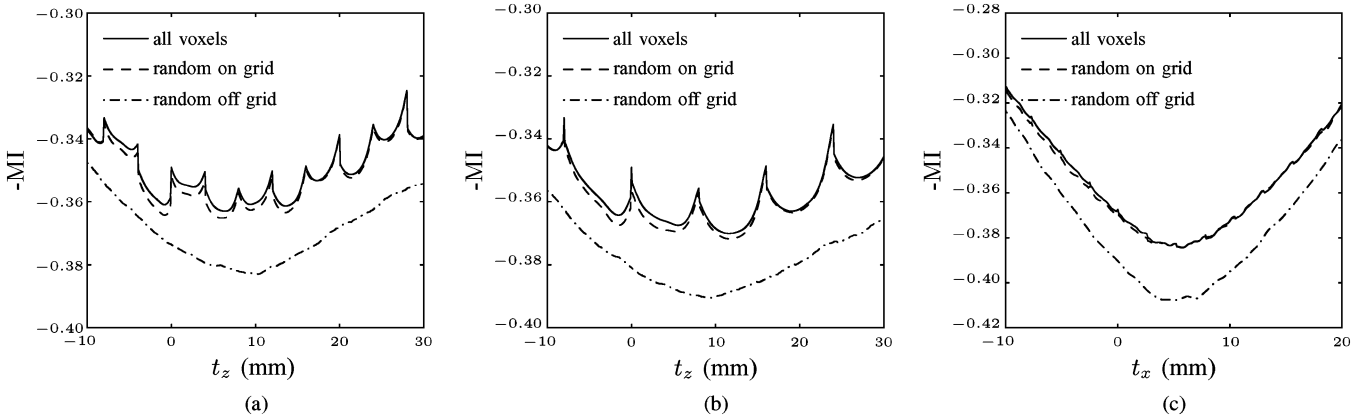

Fig. 4. Effect of different sampling strategies on the smoothness of the cost function; a) translation in the z direction; b) translation in the z direction after downsampling the MR image in the z direction; c) translation in the x direction.

was used to assess the median differences between adjacent columns. A star on top of a column indicates a significant difference $(p < 0.05)$ with respect to the previous column. The graph clearly shows that a nonrigid registration was essential in this application. The best results were obtained using a *B*-spline control point spacing of 8 mm. Refining the control point spacing to 4 mm yielded worse results due to a lack of regularization. The transformation had too many degrees-of-freedom in this case, which caused unrealistic deformations. The outlier with a very low DSC value represents a case where the translation registration failed completely. The subsequent nonrigid registration was not able to recover from this error. With the optimal setting of 8 mm, the computation time was around 15 min per registration on a single processor Pentium 2.8-GHz personal computer.

B. Sampling Strategies

The grid effect is a well-known issue in image registration. It refers to the problem that the cost function contains irregularities at locations representing grid-aligning transformations, which can impede the registration process. It has often been studied in the context of interpolation artefacts [25]. In this section it is demonstrated that the sampling mechanism can solve this issue, by taking samples off the voxel grid, as suggested in [57], [58].

Brain images were taken from the "retrospective image registration evaluation" (RIRE) project [27], which has ground truth correspondences for the 8 corner points of the images. We investigated the registration of a T1-weighted MR image (moving image) to a PET image (both of patient 001). The PET image had a dimension of $128 \times 128 \times 15$ voxels of size $2.59 \times 2.59 \times 8.0$ mm. The MR image had a dimension of $256 \times 256 \times 26$ voxels of size $1.25 \times 1.25 \times 4.0$ mm.

The cost function (MI) was analysed using an exhaustive search in a single translation direction, with a step size of 0.1 mm. Linear interpolation was used to compute $I_M(\boldsymbol{T}_{\boldsymbol{\mu}}(\boldsymbol{x}))$. Different sampling strategies were employed for computing the cost function: all voxels, random sampling on the voxel grid, and random sampling off the voxel grid.

In Fig. 4(a) the cost function $-\mathrm{MI}(\boldsymbol{T}_{\boldsymbol{\mu}}; I_F, I_M)$ is plotted as a function of the translation t_z, the direction with the largest voxel spacing. The two samplers that take samples on the voxel grid have a very irregular cost function. The irregularities show a pattern, related to the voxel sizes of the images in the z direction (8 mm for PET, 4 mm for MR). Every 8 mm a slice of the PET image maps outside the MR image. This causes the large discontinuities at $t_z = 12$ mm and 20 mm for example. Every 4 mm, the cost function exhibits a small local maximum, caused by the aligning voxel grids of the images. The random sampler that takes samples off the grid clearly leads to a much smoother cost function.

The experiment was repeated after downsampling the MR image by a factor of 2 in the z direction. The slice distance of the MR image thus became equal to that of the PET image (8 mm). Fig. 4(b) shows the cost function as a function of t_z. The irregularities follow a single pattern in this graph, with a peak at every 8 mm.

Fig. 4(c) shows the result for translation in the x direction (obtained using the original nondownsampled MR image). The portion of voxels of the PET image that move simultaneously outside the MR image domain is smaller than in the z direction. Consequently, the grid effect is reduced. The cost function appears much smoother, also for the two samplers that take samples on the voxel grid, although small irregularities remain visible at multiples of the voxel spacing. This example shows that, in practice, it may not always be strictly necessary to sample voxels off the grid. The latter suggestion is confirmed by performing a full rigid registration using the adaptive stochastic gradient descent optimization routine [55] on six patients from the RIRE database. The RIRE website reports mean errors of 2.71 and 2.78 mm for random sampling on and off the grid, respectively.

C. Multiresolution Strategies

The influence of the choice of multiresolution strategy is examined in this section. CT chest scans of 26 patients were taken from a lung cancer screening trial [61]. Each patient had a baseline and a follow-up scan, acquired 3–9 months apart. The scans were obtained at full inspiration and without contrast injection on a 16-detector-row scanner (Mx8000 IDT or Brilliance 16P, Philips Medical Systems, Best, The Netherlands). Images were of size 512×512 pixels in-plane, with the pixel size ranging from 0.55×0.55 mm to 0.8×0.8 mm. The number of slices varied from 383 to 529, with slice thickness 1 mm and slice

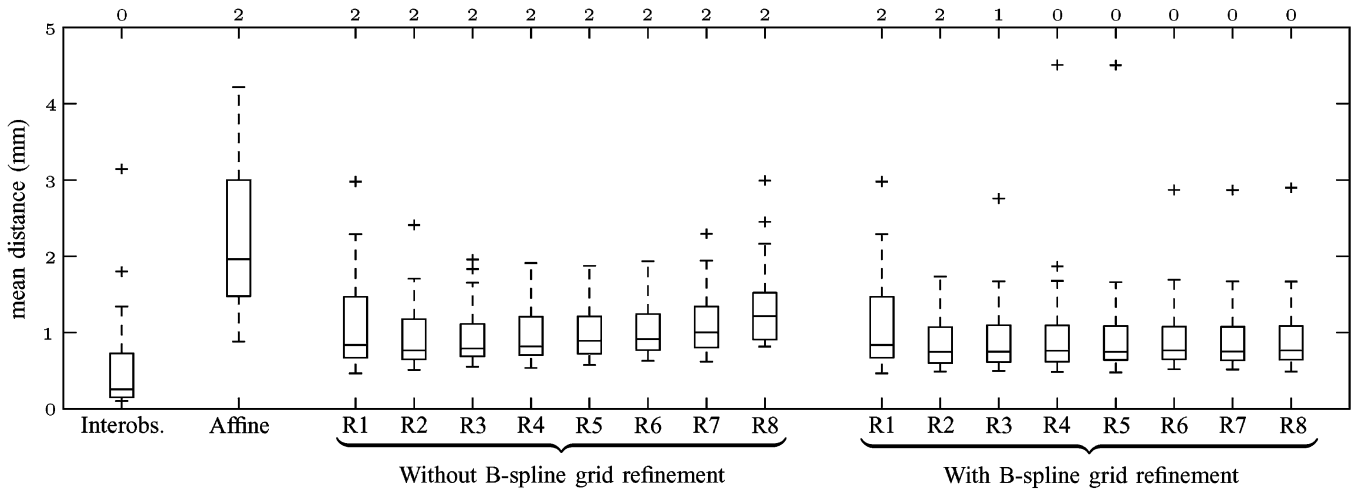

Fig. 5. Effect of the multiresolution strategy on registration accuracy, expressed as the mean distance between corresponding points. "R1"–"R8" refer to the number of image resolution levels that was used. The numbers on top of the graph refer to the number of outliers with mean distance larger than 5 mm.

spacing 0.7 mm. The images were downsampled by a factor of two in each dimension before registration, in order to decrease computational load.

For each patient the baseline and follow-up scans were registered using a nonrigid *B*-spline transformation. An affine registration was used for initialization. The registration was performed with a Gaussian image pyramid (without downsampling) using $R \in \{1, \ldots, 8\}$ levels. Two experiments were performed for each value of R. Firstly, the resolution of the *B*-spline control point grid was kept at a constant value of 12 mm (isotropic) in all resolutions. Secondly, the grid was refined after each resolution, such that at the final resolution the control points were spaced 12 mm apart again. This yields 16 experiments on 26 image pairs, resulting in a total of 416 registrations. For the cost function MI was used. The Robbins–Monro stochastic optimization method was applied, using 1000 iterations per resolution level. The image sampler was configured to select 2000 samples randomly in each iteration.

One hundred corresponding points in each baseline and follow-up scan were established by two independent observers using a semi-automatic algorithm [62]. The transformation $\boldsymbol{T}_{\hat{\boldsymbol{\mu}}}$ was applied to the annotated points in the fixed image using `transformix`. To evaluate the registration accuracy, the mean distance between the resulting locations and the reference standard of the observer annotations was computed.

Fig. 5 shows box-and-whisker plots of the mean distance to the annotations of one of the observers. The interobserver variability is shown in the left-most column. The first group R1–R8 displays the results without grid refinement. The second group shows the results with grid refinement. When no grid refinement was used, the registration quality improved until $R = 3$, but deteriorated for $R > 3$. Apparently, the dense *B*-spline grid yielded too much freedom on the heavily smoothed images. With grid refinement the results kept improving with increasing R up to $R = 6$ (note the decreasing number of outliers above 5 mm). In practice, when considering the computation time, three or four resolutions with grid refinement seems to be a reasonable choice. With these settings the runtime was about 10 min on an AMD Opteron running at 2.4 GHz.

IV. Guidelines

To facilitate parameter file design for starting `elastix`-users, this section provides some guidelines for choosing registration components and their configuration. It should be noted that many settings are application-dependent, and therefore it is not always possible to define proper default values.

As a starting point, default parameter files can be obtained from the parameter file database. For each component in Fig. 1 we suggest the following rules of thumb:

Cost function: Mutual information performs well for a large number of applications. Although sometimes (slightly) better results can be obtained with NC or SSD for monomodal image registration problems, MI can be considered a good default.

Transformation: Perform a rigid or affine registration prior to a nonrigid one, for better initialization. The recommended nonrigid transformation is the *B*-spline, because it is relatively fast due to its compact support, and has some inherent smoothness due to its differentiability. The control point grid spacing depends on the expected complexity of the deformation. Start tuning with a relatively coarse grid. The finer the grid, the more likely a regularization term needs to be added to the cost function.

Optimization: The adaptive stochastic gradient descent (ASGD) optimizer has good convergence properties and is relatively fast in combination with a random sampling strategy. Additionally, compared to a standard stochastic gradient descent method, some difficult application-dependent settings are estimated automatically [55].

Sampling strategies: Use a strategy that samples randomly, either on or off the voxel grid, see also Section III-B. Two thousand samples are usually enough for good performance [24]. Additionally, the use of masks can be important. Masks can be used to select a region of interest or to avoid the undesired alignment of artificial edges in the images (e.g. the cylindrical reconstruction field-of-view of CT scanners, the conic beam edge in ultrasound images, or image artifacts).

Interpolation: A first order *B*-spline (linear) interpolator offers a good trade-off between quality and computation time.

Hierarchical strategies: For the image data a Gaussian pyramid with downsampling is recommended. When sufficient computer memory is available the Gaussian pyramid without downsampling sometimes offers better results. For the nonrigid transformation model a multi-grid approach is advised. By default the grid spacing is halved every resolution level. Three or four resolutions are often sufficient; use five or six for large images with substantial deformations.

Once again we want to emphasise that the above rules are very general and will not apply to every situation.

V. Discussion

The three experiments presented in Section III are meant to demonstrate the variety of comparative parameter investigations that can be performed with elastix. Note that the conclusions drawn could be different for different medical applications. For example, the optimum *B*-spline control point resolution of 8 mm found in Section III-A can obviously not be generalized to other applications. On images with different characteristics (modality, anatomical region), new optimal parameters need to be determined. The elastix software is meant to streamline this process. An important facilitator of this is the parameter file database. Being a central storage place for elastix parameter files, it allows researchers to reproduce experiments published in literature with exactly the same settings as used in the publication.

Several other software packages that perform image registration are available on the internet, for example: AIR,[3] ART,[4] ANTS,[5], bUnwarpJ,[6] DROP,[7] FNIRT,[8] HAMMER,[9] IRTK,[10] and SPM.[11] In [63] an evaluation framework for nonrigid image registration is proposed and applied to 6 registration methods, on intersubject MR brain data. The authors derive several criteria, which can be used to evaluate and compare (nonrigid) registration algorithms. More recently, a fairly complete overview of image registration software is given in [64], which compares the performance of 14 nonrigid registration programs on MR brain images. In that article, the authors recommend, regarding software design, "where possible creating separable components for the similarity measure, transformation model, regularization method, and optimization strategy." The modular design of elastix, which makes it so suitable for comparative studies, distinguishes it from most other available image registration packages. The two-layer source code setup (see Section II-B) plays an important role in this. Other discriminating features of elastix are 1) the large choice of optimization methods, among others the efficient stochastic optimization methods described in [24], [55], 2) the various image sampling strategies, 3) the support for combining multiple transformations by composition or summation, and 4) the exhaustive possibilities for specifying any type of hierarchical strategy. Comparing the performance of software packages is not a trivial task, since each program has its own set of user-defined parameters, which may heavily influence the performance. Open challenges, such as recently organized for liver segmentation [65] and coronary artery centerline extraction [66], would be an interesting way to compare image registration software.

Several functional extensions of the elastix package could be imagined, but of highest interest would be the implementation of other nonrigid transformation models, besides the current *B*-spline transformation and the physical model based splines. Parameterized transformation models, such as described in [32], [36], [37], are easiest to integrate in the scheme of Fig. 1. Nonparametric registration methods, such as [34], [35], [38], [39], would require some more effort, but several of these algorithms have already been implemented in the ITK library (or in other ITK-based registration software, such as ANTS), which simplifies their integration in elastix.

VI. Conclusion

We have developed and presented a software package, elastix, for medical image registration. Rather than implementing a single registration method, elastix is a collection of parametric intensity-based registration methods. Thanks to the modular design, the user can easily construct a registration algorithm, tailored to a specific application. Configuration of the registration method can be accomplished by writing a few lines in a parameter text file, without having to write any programming code. elastix has a command-line interface, which simplifies batch-processing of large numbers of data sets. Registration of large 3-D images can be done efficiently, thanks to the use of stochastic subsampling techniques.

The usage of elastix has been illustrated with three experiments. In the first experiment, eight transformation models were compared for the interpatient registration of 50 MR prostate scans. In the second experiment, we reproduced a result from the literature, showing that the so-called grid effect can be reduced by sampling the fixed image off the voxel grid. The third experiment demonstrated the importance of choosing a suitable hierarchical (multiresolution) strategy, by registering 26 chest CT image pairs with 16 different multiresolution configurations. These three investigations are just a few examples of the many possible comparative studies that one can perform with elastix.

The software has been used in several research projects, including [2], [8], [15], [24], [50], [55], [67]–[73], and is still under active development. A complete list of references can be found at http://elastix.isi.uu.nl/elastixpapers.php. Both the executables and the source code are publicly available, which fits in the current trend in medical imaging towards open source software. The source code provides the users with the exact construction of the available algorithms, and allows them to enhance the functionality of elastix by adding their own al-

[3]http://air.bmap.ucla.edu.

[4]http://www.nitrc.org/projects/art.

[5]http://picsl.upenn.edu/ANTS.

[6]http://biocomp.cnb.csic.es/~iarganda/bUnwarpJ.

[7]http://www.mrf-registration.net.

[8]http://www.fmrib.ox.ac.uk/fsl/fnirt.

[9]https://www.rad.upenn.edu/sbia/projects/3-D_hammer.html.

[10]http://www.doc.ic.ac.uk/~dr/software.

[11]http://www.fil.ion.ucl.ac.uk/spm.

gorithms. These features make `elastix` a useful tool for research on medical image registration.

APPENDIX
`elastix` USAGE EXAMPLE

`elastix` is a command-line program and therefore has no graphical user interface. A list of all mandatory and optional command line arguments can be generated by calling `elastix - -help`. The most basic command to run a registration is as follows:

```
elastix -f fix.ext -m mov.ext -out outDir -p
par.txt
```

Here, `fix` and `mov` are I_F and I_M, respectively, and `ext` is a supported extension for image file formats. All output, e.g., log-files, $\hat{\boldsymbol{\mu}}$, the deformed moving image $I_M(\boldsymbol{T}_{\hat{\boldsymbol{\mu}}}(\boldsymbol{x}))$, is written in the directory `outDir`. The parameter file `par.txt` specifies which components are selected and what their parameters are. A part of it could look like

```
(Metric "AdvancedMattesMutualInformation")
(Optimizer "StandardGradientDescent")
(Transform "EulerTransform")

(NumberOfResolutions 3)

//Mutual information specific:
(NumberOfHistogramBins 32)
(FixedKernelBSplineOrder 1)
(MovingKernelBSplineOrder 3)

//Optimizer specific: stepsize a_k =
a/(A + k + 1)^alpha

(MaximumNumberOfIterations 300 300 600)
(SP_a 0.001)
(SP_alpha 0.602)
(SP_A 50.0)
```

For more detailed information about calling `elastix` and the structure of the parameter file we refer to the manual, Chapter 3 and Appendix A.

ACKNOWLEDGMENT

The authors thank Dr. U. A. van der Heide for providing the prostate MR scans and Dr. M. van Vulpen for the manual prostate segmentations.

REFERENCES

[1] D. Mattes, D. R. Haynor, H. Vesselle, T. K. Lewellen, and W. Eubank, "PET-CT image registration in the chest using free-form deformations," *IEEE Trans. Med. Imag.*, vol. 22, no. 1, pp. 120–128, Jan. 2003.

[2] M. Staring, S. Klein, and J. P. W. Pluim, "A rigidity penalty term for nonrigid registration," *Med. Phys.*, vol. 34, no. 11, pp. 4098–4108, 2007.

[3] D. Rueckert, L. I. Sonoda, and C. Hayes *et al.*, "Nonrigid registration using free-form deformations: Application to breast MR images," *IEEE Trans. Med. Imag.*, vol. 18, no. 8, pp. 712–721, Aug. 1999.

[4] T. Rohlfing, C. R. Maurer, Jr., D. A. Bluemke, and M. A. Jacobs, "Volume-preserving nonrigid registration of MR breast images using free-form deformation with an incompressibility constraint," *IEEE Trans. Med. Imag.*, vol. 22, no. 6, pp. 730–741, Jun. 2003.

[5] M. Foskey, B. Davis, and L. Goyal *et al.*, "Large deformation three-dimensional image registration in image-guided radiation therapy," *Phys. Med. Biol.*, vol. 50, pp. 5869–5892, 2005.

[6] X. Pennec, P. Cachier, and N. Ayache, "Tracking brain deformations in time sequences of 3-D US images," *Pattern Recognit. Lett.*, vol. 24, no. 4–5, pp. 801–813, 2003.

[7] T. Rohlfing, R. Brandt, R. Menzel, and C. R. Maurer, Jr., "Evaluation of atlas selection strategies for atlas-based image segmentation with application to confocal microscopy images of bee brains," *NeuroImage*, vol. 21, no. 4, pp. 1428–1442, 2004.

[8] S. Klein, U. A. van der Heide, and I. M. Lips *et al.*, "Automatic segmentation of the prostate in 3-D MR images by atlas matching using localized mutual information," *Med. Phys.*, vol. 35, no. 4, pp. 1407–1417, Apr. 2008.

[9] R. A. Heckemann, J. V. Hajnal, P. Aljabar, D. Rueckert, and A. Hammers, "Automatic anatomical brain MRI segmentation combining label propagation and decision fusion," *NeuroImage*, vol. 33, no. 1, pp. 115–126, 2006.

[10] S. Maheswaran, H. Barjat, and S. T. Bate *et al.*, "Analysis of serial magnetic resonance images of mouse brains using image registration," *NeuroImage*, vol. 44, no. 3, pp. 692–700, 2009.

[11] C. Baillard, P. Hellier, and C. Barillot, "Segmentation of brain 3-D MR images using level sets and dense registration," *Med. Image Anal.*, vol. 5, no. 3, pp. 185–194, 2001.

[12] W. R. Crum, R. I. Scahill, and N. C. Fox, "Automated hippocampal segmentation by regional fluid registration of serial MRI: Validation and application in alzheimer's disease," *NeuroImage*, vol. 13, no. 5, pp. 847–855, 2001.

[13] L. Zhang, E. A. Hoffman, and J. M. Reinhardt, "Atlas-driven lung lobe segmentation in volumetric X-ray CT images," *IEEE Trans. Med. Imag.*, vol. 25, no. 1, pp. 1–16, Jan. 2006.

[14] T. A. Sundaram and J. C. Gee, "Towards a model of lung biomechanics: Pulmonary kinematics via registration of serial lung images," *Med. Image Anal.*, vol. 9, no. 6, pp. 524–537, 2005.

[15] H. A. Vrooman, C. A. Cocosco, and F. van der Lijn *et al.*, "Multi-spectral brain tissue segmentation using automatically trained k-nearest-neighbor classification," *NeuroImage*, vol. 37, no. 1, pp. 71–81, 2007.

[16] P. Anbeek, K. L. Vincken, M. J. P. van Osch, R. H. C. Bisschops, and J. van der Grond, "Automatic segmentation of different-sized white matter lesions by voxel probability estimation," *Med. Image Anal.*, vol. 8, no. 3, pp. 205–215, 2004.

[17] L. G. Brown, "A survey of image registration techniques," *ACM Comput. Surv.*, vol. 24, no. 4, pp. 325–376, 1992.

[18] J. B. A. Maintz and M. A. Viergever, "A survey of medical image registration," *Medical Image Analysis*, vol. 2, no. 1, pp. 1–36, 1998.

[19] H. Lester and S. R. Arridge, "A survey of hierarchical non-linear medical image registration," *Pattern Recognit.*, vol. 32, no. 1, pp. 129–149, 1999.

[20] D. Hill, P. G. Batchelor, M. Holden, and D. J. Hawkes, "Medical image registration," *Phys. Med. Biol.*, vol. 46, no. 3, pp. R1–R45, 2001.

[21] J. Modersitzki, *Numerical Methods for Image Registration*. New York: Oxford Univ. Press, 2004.

[22] A. Gholipour, N. Kehtarnavaz, R. Briggs, M. Devous, and K. Gopinath, "Brain functional localization: A survey of image registration techniques," *IEEE Trans. Image Process.*, vol. 26, no. 4, pp. 427–451, Apr. 2007.

[23] F. Maes, D. Vandermeulen, and P. Suetens, "Comparative evaluation of multiresolution optimization strategies for multimodality image registration by maximization of mutual information," *Med. Image Anal.*, vol. 3, no. 4, pp. 373–386, 1999.

[24] S. Klein, M. Staring, and J. P. W. Pluim, "Evaluation of optimization methods for nonrigid medical image registration using mutual information and B-splines," *IEEE Trans. Image Process.*, vol. 16, no. 12, pp. 2879–2890, Dec. 2007.

[25] J. P. W. Pluim, J. B. A. Maintz, and M. A. Viergever, "Interpolation artefacts in mutual information-based image registration," *Comput. Vis. Image Understand.*, vol. 77, no. 2, pp. 211–232, 2000.

[26] P. Viola and W. M. Wells, III, "Alignment by maximization of mutual information," *Int. J. Comput. Vis.*, vol. 24, no. 2, pp. 137–154, 1997.

[27] J. West, J. M. Fitzpatrick, and M. Y. Wang *et al.*, "Comparison and evaluation of retrospective intermodality brain image registration techniques," *J. Comput. Assist. Tomogr.*, vol. 21, no. 4, pp. 554–566, 1997.

[28] F. L. Bookstein, "Principal warps: Thin-plate splines and the decomposition of deformations," *IEEE Trans. Pattern Anal. Mach. Intell.*, vol. 11, no. 6, pp. 567–585, Jun. 1989.

[29] R. Bajcsy and S. Kovačič, "Multiresolution elastic matching," *Comput. Vis. Graphics Image Process.*, vol. 46, no. 1, pp. 1–21, 1989.

[30] M. H. Davis, A. Khotanzad, D. P. Flamig, and S. E. Harms, "A physics-based coordinate transformation for 3-D image matching," *IEEE Trans. Med. Imag.*, vol. 26, no. 3, pp. 317–328, Jun. 1997.

[31] J. Gee, "On matching brain volumes," *Pattern Recognit.*, vol. 32, no. 1, pp. 99–111, 1999.
[32] G. K. Rohde, A. Aldroubi, and B. M. Dawant, "The adaptive bases algorithm for intensity-based nonrigid image registration," *IEEE Trans. Med. Imag.*, vol. 22, no. 11, pp. 1470–1479, Nov. 2003.
[33] E. D'Agostino, F. Maes, D. Vandermeulen, and P. Suetens, "A viscous fluid model for multimodal non-rigid image registration using mutual information," *Med. Image Anal.*, vol. 7, no. 4, pp. 565–575, 2003.
[34] B. Avants and J. C. Gee, "Geodesic estimation for large deformation anatomical shape averaging and interpolation," *NeuroImage*, vol. 23, pp. S139–S150, 2004.
[35] B. Fischer and J. Modersitzki, "A unified approach to fast image registration and a new curvature based registration technique," *Linear Algebra Appl.*, vol. 380, pp. 107–124, 2004.
[36] V. Arsigny, X. Pennec, and N. Ayache, "Polyrigid and polyaffine transformations: A novel geometrical tool to deal with non-rigid deformations—Application to the registration of histological slices," *Med. Image Anal.*, vol. 9, no. 6, pp. 507–523, 2005.
[37] A. du Bois d'Aische, M. D. Craene, and X. Geets *et al.*, "Efficient multi-modal dense field non-rigid registration: Alignment of histological and section images," *Med. Image Anal.*, vol. 9, no. 6, pp. 538–546, 2005.
[38] F. Beg, M. Miller, A. Trouve, and L. Younes, "Computing large deformation metric mappings via geodesic flows of diffeomorphisms," *Int. J. Comput. Vis.*, vol. 61, no. 2, pp. 139–157, 2005.
[39] T. Vercauteren, X. Pennec, A. Perchant, and N. Ayache, "Diffeomorphic demons: Efficient non-parametric image registration," *NeuroImage*, vol. 45, pp. S61–S72, 2009.
[40] P. Thévenaz, U. E. Ruttimann, and M. Unser, "A pyramid approach to subpixel registration based on intensity," *IEEE Trans. Image Process.*, vol. 7, no. 1, pp. 27–41, Jan. 1998.
[41] J. Kybic and M. Unser, "Fast parametric elastic image registration," *IEEE Trans. Image Process.*, vol. 12, no. 11, pp. 1427–1442, Nov. 2003.
[42] C. Studholme, D. L. G. Hill, and D. J. Hawkes, "Automated 3-D registration of MR and CT images of the head," *Med. Image Anal.*, vol. 1, no. 2, pp. 163–175, 1996.
[43] G. P. Penney, J. Weese, and J. A. Little *et al.*, "A comparison of similarity measures for use in 2-D-3-D medical image registration," *IEEE Trans. Med. Imag.*, vol. 17, no. 4, pp. 586–595, Aug. 1998.
[44] F. Maes, A. Collignon, D. Vandermeulen, G. Marchal, and P. Suetens, "Multimodality image registration by maximization of mutual information," *IEEE Trans. Med. Imag.*, vol. 16, no. 2, pp. 187–198, Apr. 1997.
[45] P. Thévenaz and M. Unser, "Optimization of mutual information for multiresolution image registration," *IEEE Trans. Image Process.*, vol. 9, no. 12, pp. 2083–2099, Dec. 2000.
[46] J. P. W. Pluim, J. B. A. Maintz, and M. A. Viergever, "Mutual-information-based registration of medical images: A survey," *IEEE Trans. Med. Imag.*, vol. 22, no. 8, pp. 986–1004, Aug. 2003.
[47] C. Studholme, D. L. G. Hill, and D. J. Hawkes, "An overlap invariant entropy measure of 3-D medical image alignment," *Pattern Recognit.*, vol. 32, no. 1, pp. 71–86, 1999.
[48] L. Ibáñez, W. Schroeder, L. Ng, and J. Cates, *The ITK Software Guide*, 2nd ed. Clifton Park, NY: Kitware, 2005.
[49] H. Neemuchwala and A. Hero, *Entropic Graphs for Registration*, ser. Signal Processing and Communications. New York: CRC Press, 2005, ch. 6, pp. 185–235.
[50] M. Staring, U. A. van der Heide, S. Klein, M. A. Viergever, and J. P. W. Pluim, "Registration of cervical MRI using multifeature mutual information," *IEEE Trans. Med. Imag.*, vol. 28, no. 9, pp. 1412–1421, Sep. 2009.
[51] A. P. Zijdenbos, B. M. Dawant, R. A. Margolin, and P. A. C. , "Morphometric analysis of white matter lesions in MR images: Method and validation," *IEEE Trans. Med. Imag.*, vol. 13, no. 4, pp. 716–724, Dec. 1994.
[52] R. Brooks and T. Arbel, "Improvements to the itk::KernelTransform and subclasses," *Insight J.* Jan.–Jun. 2007 [Online]. Available: http://hdl.handle.net/1926/494
[53] M. Unser, "Splines: A perfect fit for signal and image processing," *IEEE Signal Process. Mag.*, vol. 16, no. 6, pp. 22–38, Nov. 1999.
[54] D. Rueckert, A. F. Frangi, and J. A. Schnabel, "Automatic construction of 3-D statistical deformation models of the brain using non-rigid registration," *IEEE Trans. Med. Imag.*, vol. 22, no. 8, pp. 1014–1025, Aug. 2003.
[55] S. Klein, J. P. W. Pluim, M. Staring, and M. A. Viergever, "Adaptive stochastic gradient descent optimisation for image registration," *Int. J. Comput. Vis.*, vol. 81, no. 3, pp. 227–239, 2009.
[56] R. Bhagalia, J. A. Fessler, and B. Kim, "Accelerated nonrigid intensity-based image registration using importance sampling," *IEEE Trans. Med. Imag.*, vol. 28, no. 8, pp. 1208–1216, Aug. 2009.
[57] B. Likar and F. Pernuš, "A hierarchical approach to elastic registration based on mutual information," *Image Vision Comput.*, vol. 19, no. 1–2, pp. 33–44, 2001.
[58] P. Thévenaz, M. Bierlaire, and M. Unser, "Halton sampling for image registration based on mutual information," *Sampling Theory Signal Image Process.*, vol. 7, no. 2, pp. 141–171, 2008.
[59] P. Thévenaz, T. Blu, and M. Unser, "Interpolation revisited," *IEEE Trans. Med. Imag.*, vol. 19, no. 7, pp. 739–758, Jul. 2000.
[60] L. R. Dice, "Measures of the amount of ecologic association between species," *Ecology*, vol. 26, no. 3, pp. 297–302, 1945.
[61] C. A. van Iersel, H. J. de Koning, and G. Draisma *et al.*, "Risk-based selection from the general population in a screening trial: Selection criteria, recruitment and power for the Dutch-Belgian randomised lung cancer multi-slice CT screening trial (NELSON)," *Int. J. Cancer*, vol. 120, no. 4, pp. 868–874, 2007.
[62] K. Murphy, B. van Ginneken, J. P. W. Pluim, S. Klein, and M. Staring, "Semi-automatic reference standard construction for quantitative evaluation of lung CT registration," in *MICCAI*, 2008, vol. 5242, Lecture Notes in Computer Science, pp. 1006–1013.
[63] P. Hellier, C. Barillot, and I. Corouge *et al.*, "Retrospective evaluation of intersubject brain registration," *IEEE Trans. Med. Imag.*, vol. 22, no. 9, pp. 1120–1130, Sep. 2003.
[64] A. Klein, J. Andersson, and B. A. Ardekani *et al.*, "Evaluation of 14 nonlinear deformation algorithms applied to human brain MRI registration," *NeuroImage*, vol. 46, pp. 786–802, 2009.
[65] T. Heimann, B. van Ginneken, and M. Styner *et al.*, "Comparison and evaluation of methods for liver segmentation from CT datasets," *IEEE Trans. Med. Imag.*, vol. 28, no. 8, pp. 1251–1265, Aug. 2009.
[66] M. Schaap, C. T. Metz, and T. van Walsum *et al.*, "Standardized evaluation methodology and reference database for evaluating coronary artery centerline extraction algorithms," *Med. Image Anal.*, vol. 13, no. 5, pp. 701–714, 2009.
[67] M. Staring, S. Klein, and J. P. W. Pluim, "Nonrigid registration with tissue-dependent filtering of the deformation field," *Phys. Med. Biol.*, vol. 52, no. 23, pp. 6879–6892, 2007.
[68] E. M. van Rikxoort, Y. Arzhaeva, and B. van Ginneken, "A multi-atlas approach to automatic segmentation of the caudate nucleus in MR brain images," in *3-D Segmentation in the Clinic: A Grand Challenge*, T. Heimann, M. Styner, and B. van Ginneken, Eds., 2007, pp. 29–36 [Online]. Available: http://mbi.dkfz-heidelberg.de/grand-challenge2007
[69] B. Glocker, N. Komodakis, G. Tziritas, N. Navab, and N. Paragios, "Dense image registration through MRFs and efficient linear programming," *Med. Image Anal.*, vol. 12, no. 6, pp. 731–741, 2008.
[70] A. Hurvitz and L. Joskowicz, "Registration of a CT-like atlas to fluoroscopic X-ray images using intensity correspondences," *Int. J. Comput. Assist. Radiol. Surg.*, vol. 3, no. 6, pp. 493–504, 2008.
[71] F. van der Lijn, T. den Heijer, M. M. B. Breteler, and W. J. Niessen, "Hippocampus segmentation in MR images using atlas registration, voxel classification, and graph cuts," *NeuroImage*, vol. 43, no. 4, pp. 708–720, 2008.
[72] Y. Yin, E. A. Hoffman, and C.-L. Lin, "Mass preserving nonrigid registration of CT lung images using cubic B-spline," *Med. Phys.*, vol. 36, no. 9, pp. 4213–4222, 2009.
[73] X. Artaechevarria, A. Munoz-Barrutia, and C. O. de Solorzano, "Combination strategies in multi-atlas image segmentation: Application to brain MR data," *IEEE Trans. Med. Imag.*, vol. 28, no. 8, pp. 1266–1277, Aug. 2009.